J Eng Math (2009) 63:155–176
DOI 10.1007/s10665-008-9226-2

Asymptotic and numerical analysis of a simple model for blade coating

Judit Quintans Carou · Stephen K. Wilson · Nigel J. Mottram · Brian R. Duffy

Received: 3 July 2007 / Accepted: 13 March 2008 / Published online: 12 April 2008

Abstract Motivated by the industrial process of blade coating, the two-dimensional flow of a thin film of Newtonian fluid on a horizontal substrate moving parallel to itself with constant speed under a fixed blade of finite length in which the flows upstream and downstream of the blade are coupled via the flow under the blade is analysed. A combination of asymptotic and numerical methods is used to investigate the number and nature of the steady solutions that exist. Specifically, it is found that in the presence of gravity there is always at least one, and (depending on the parameter values) possibly as many as three, steady solutions, and that when multiple solutions occur they are identical under and downstream of the blade, but differ upstream of it. The stability of these solutions is investigated, and their asymptotic behaviour in the limits of large and small flux and weak and strong gravity effects, respectively, determined.

Keywords Asymptotics · Blade coating · Thin-film flow

1 Introduction

During the industrial process of blade coating, a thin fluid film is applied to a moving substrate by the action of a fixed blade (or vice versa). Blade coating is important because of the wide range of products in whose manufacture it is used, including newspapers and catalogues, photographic films, magnetic storage media and fibres. The economic importance of this process has motivated extensive research in order to understand better the underlying physical mechanisms involved, and hence to improve its efficiency. In particular, various mathematical models for blade coating have been developed in order to predict the form and thickness of the final coated film. Ruschak [1] reviews some of the early mathematical work on various fluid coating processes, and a more recent account of the large and growing literature on coating can be found in the encyclopaedic volume edited by Kistler and Schweizer [2]. Regular scientific conferences on coating in Europe (the European Coating Symposium: see, for example, [3]) and the USA (the International Coating Science and Technology Symposium, [4]) attest to the ongoing interest and research activity in this area.

In the present paper we analyse a simple model of the blade-coating process consisting of the two-dimensional flow of a thin film of Newtonian fluid on a horizontal substrate moving parallel to itself with constant speed under

J. Quintans Carou · S. K. Wilson (✉) · N. J. Mottram · B. R. Duffy
Department of Mathematics, University of Strathclyde, Livingstone Tower, 26 Richmond Street, Glasgow G1 1XH, UK
e-mail: s.k.wilson@strath.ac.uk

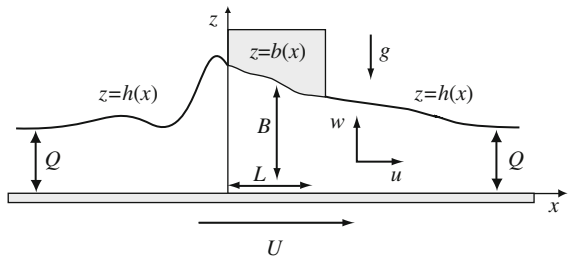

Fig. 1 Steady, two-dimensional flow of a thin film of Newtonian fluid on a horizontal substrate moving parallel to itself with constant speed U under a fixed blade of finite length L

a fixed blade of finite length in which the flows upstream and downstream of the blade are coupled via the flow under the blade.

The starting point for the present analysis is the work of Moriarty and Terrill [5] who investigated the same problem in the special case of a horizontal blade in the absence of gravity, as an idealised model for the motion of a hard contact lens on the tear film in the human eye. In particular, for their problem Moriarty and Terrill [5] predicted the existence of none, one or two steady solutions, and in an associated paper McLeod [6] proved analytically the existence and multiplicity of these solutions.

In the present paper we build on the work of Moriarty and Terrill [5] by using a combination of asymptotic and numerical methods to show that accounting for the presence of gravity has a significant effect on the number and nature of the steady solutions that exist. Specifically, we find that in this case there is always at least one, and (depending on the parameter values) possibly as many as three, steady solutions, and that when multiple solutions occur they are identical under and downstream of the blade, but differ upstream of it. We discuss the stability of these solutions, and determine their asymptotic behaviour in the limits of large and small flux and weak and strong gravity effects, respectively.

2 The mathematical model

2.1 Formulation

We consider steady, two-dimensional flow of a thin film of Newtonian fluid of constant density ρ, viscosity μ and surface-tension coefficient γ on a horizontal substrate which is taken to lie in the plane $z = 0$ and is moving parallel to itself with constant speed U (>0) in the positive x-direction, where xyz are Cartesian coordinates. The fluid has a free surface $z = h(x)$, except where it flows underneath a fixed blade of finite length L and prescribed shape $z = b(x)$ in $0 \le x \le L$, as shown in Fig. 1. The velocity $\mathbf{v}$ and pressure p are written as $\mathbf{v} = \mathbf{v}(x, z) = (u(x, z), 0, w(x, z))$ and $p = p(x, z)$, and gravity acts in the negative z-direction. We use the following non-dimensionalisations:

$$x = Lx^*, \quad z = Bz^*, \quad b = Bb^*, \quad b_0 = Bb_0^*, \quad b_L = Bb_1^*, \quad h = Bh^*,$$
$$u = Uu^*, \quad w = \frac{BU}{L}w^*, \quad p - p_\mathrm{a} = \frac{\mu UL}{B^2}p^*, \quad Q = UBQ^*, \tag{1}$$

where B is a typical film thickness, $b_0 = b(0)$ and $b_L = b(L)$ denote the heights of the blade at $x = 0$ and $x = L$, respectively, p_a is the constant atmospheric pressure, and Q is the constant volume flux of fluid (per unit width) in the x direction, given by

$$Q = \begin{cases} \displaystyle\int_0^b u \, \mathrm{d}z & \text{for } 0 \le x \le L, \\ \displaystyle\int_0^h u \, \mathrm{d}z & \text{for } x \le 0 \quad \text{and } x \ge L. \end{cases} \tag{2}$$

Henceforth we drop the superscript stars from the non-dimensional variables.

We employ a thin-film approximation (see, for example, [7, Chap. 4]) based on the assumption that the aspect ratio ϵ of the film, defined by $\epsilon = B/L$, is small, that is, $\epsilon \ll 1$. This assumption is well justified in many practical

coating situations (see, for example, [2]). In the limit $\epsilon \to 0$ the leading-order governing thin-film equations are

$$0 = u_x + w_z, \quad 0 = p_x - u_{zz}, \quad 0 = p_z + G, \tag{3,4,5}$$

where the non-dimensional gravity parameter G, given by

$$G = \frac{\rho g B^3}{\mu U L}, \tag{6}$$

is a measure of the relative strength of gravitational and viscous effects.

We assume that the free surface is pinned at the ends of the blade; therefore

$$h(0) = b_0, \quad h(1) = b_1. \tag{7,8}$$

At the ends of the blade we also impose continuity of both pressure and flux in the x-direction between the flow under the blade and the flow with a free surface. The usual no-slip and no-penetration conditions at solid boundaries and the balance of normal and tangential stresses at the free surface correspond to

$$u = 1, \quad w = 0 \quad \text{on} \quad z = 0, \tag{9}$$

$$u = 0, \quad w = 0 \quad \text{on} \quad z = b \quad \text{for} \quad 0 \le x \le 1, \tag{10}$$

$$u_z = 0, \quad p = -Sh_{xx} \quad \text{on} \quad z = h \quad \text{for} \quad x \le 0 \quad \text{and} \quad x \ge 1, \tag{11}$$

where the non-dimensional surface-tension parameter S, given by

$$S = \frac{\gamma B^3}{\mu U L^3}, \tag{12}$$

is a measure of the relative strength of surface-tension and viscous effects. In the limit $|x| \to \infty$ we assume that the fluid is in the form of a uniform layer of thickness Q (with Q prescribed a priori) which is at rest relative to the substrate, and hence

$$p_x \to 0 \quad \text{and} \quad h \to Q \quad \text{as} \quad |x| \to \infty. \tag{13}$$

Furthermore,

$$p \to p_{\infty \mathrm{L}} \quad \text{as} \quad x \to -\infty \quad \text{and} \quad p \to p_{\infty \mathrm{R}} \quad \text{as} \quad x \to +\infty, \tag{14}$$

where $p_{\infty \mathrm{L}}$ and $p_{\infty \mathrm{R}}$ are the external pressures far upstream and far downstream of the blade, respectively.

2.2 Solution

As, for example, Quintans Carou et al. [8] showed, the velocity and pressure for the flow under the blade (i.e., for $0 \le x \le 1$) can be calculated directly from (2) to (5) subject to boundary conditions (9) and (10) to be

$$u(x,z) = \frac{b-z}{b^3}\left[b^2 + 3(2Q-b)z\right], \quad w(x,z) = \frac{2(3Q-b)}{b^4} b_x (b-z) z^2, \tag{15,16}$$

$$p(x,z) = p_0 - Gz + 6I_2(x) - 12QI_3(x), \tag{17}$$

where we have defined

$$I_n(x) = \int_0^x \frac{1}{b^n(\tilde{x})}\, \mathrm{d}\tilde{x}, \tag{18}$$

and $p_0 = p(0,0)$ is an undetermined constant. The stream function ψ, defined by $u = \psi_z$ and $w = -\psi_x$, subject to $\psi(z=0) = 0$ and satisfying $\psi(z=b) = Q$, is given by

$$\psi = \frac{3(b-2Q)}{b^3}\left(\frac{z^3}{3} - \frac{bz^2}{2}\right) - \frac{z^2}{2b} + z. \tag{19}$$

The fluid velocity and pressure for the flow with a free surface (i.e., for $x \leq 0$ and $x \geq 1$) can be calculated from (3)–(5) subject to boundary conditions (9), (11) and (14) to be

$$u(x,z) = 1 - \frac{p_x}{2}(2h - z)\,z, \quad w(x,z) = \frac{p_{xx}}{6}(3h - z)\,z^2 + \frac{p_x}{2}h_x z^2, \tag{20,21}$$

$$p(x,z) = \begin{cases} p_{\infty \mathrm{L}} + G(h - z) - Sh_{xx} & \text{for } x \leq 0, \\ p_{\infty \mathrm{R}} + G(h - z) - Sh_{xx} & \text{for } x \geq 1. \end{cases} \tag{22}$$

By (2) and (20) we have

$$Q = h - \frac{p_x}{3}h^3, \tag{23}$$

and hence, using (20) and (23), we may re-write u in the form

$$u = 1 + \frac{3(Q - h)(2h - z)z}{2h^3}, \tag{24}$$

so that the curve $z = z_0$ on which $u = 0$ is given by

$$\frac{z_0}{h} = 1 - \sqrt{\frac{3Q - h}{3(Q - h)}}. \tag{25}$$

Hence, if $h > 3Q$, there is a region of reverse flow (i.e., $u < 0$) when $z_0 < z < h$ which might be undesirable in practical coating applications. The stream function ψ, subject to $\psi(z = 0) = 0$ and satisfying $\psi(z = h) = Q$, is given by

$$\psi = \frac{3(h - Q)}{2h^3}\left(\frac{z^3}{3} - hz^2\right) + z. \tag{26}$$

Substituting the solution (22) for p in (23) leads to the governing third-order ordinary differential equation for the free-surface profile h, namely

$$(Sh_{xx} - Gh)_x = \frac{3(Q - h)}{h^3}. \tag{27}$$

Imposing continuity of pressure at $x = 0$ yields

$$p_0 = p_{\infty \mathrm{L}} + Gb_0 - Sh_{xx}(0), \tag{28}$$

and imposing continuity of pressure at $x = 1$ and using (28) yields

$$p_{\infty \mathrm{L}} - p_{\infty \mathrm{R}} + G(b_0 - b_1) - S[h_{xx}(0) - h_{xx}(1)] + 6I_2(1) - 12QI_3(1) = 0, \tag{29}$$

where $I_n(x)$ is again given by (18).

The free-surface profile is determined by solving (27) subject to (7) and (13) upstream of the blade and (8) and (13) downstream of the blade, coupled via (29).

In what follows, the shape of the blade, $b(x)$, the external pressures far upstream and far downstream of the blade, $p_{\infty \mathrm{L}}$ and $p_{\infty \mathrm{R}}$, and the non-dimensional surface tension, S, remain arbitrary. However, in all the examples shown, for simplicity and definiteness we restrict our attention to the particular case of a horizontal blade $b(x) \equiv b$, where b is a constant, $p_{\infty \mathrm{L}} = p_{\infty \mathrm{R}}$, and, without loss of generality, $S = 1$ (corresponding to the choice $B = (\mu U/\gamma)^{1/3}L$).

The solution of (27) was found numerically using AUTO97, a FORTRAN-based software package for bifurcation problems involving ordinary differential equations [9], and reveals that the relative sizes of the non-dimensional surface tension S, gravity G and volume flux Q have a significant effect on the number and nature of the steady solutions that exist.

Figure 2 shows a typical G–Q parameter plane showing the number of steady solutions in the different regions when $b = 1$, $p_{\infty \mathrm{L}} = p_{\infty \mathrm{R}}$ and $S = 1$. A somewhat similar parameter plane was recently obtained by Quintans Carou et al. [10, Fig. 5] for a closely related "drag in" problem of a thin film of fluid on a horizontal substrate moving parallel to itself towards and under a fixed blade. If $G = 0$, there is a unique solution for values of Q

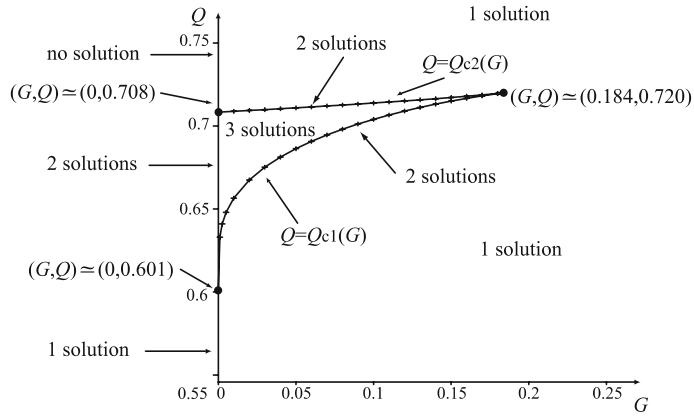

Fig. 2 Typical G–Q parameter plane showing the number of steady solutions in the different regions when $b = 1$, $p_{\infty L} = p_{\infty R}$ and $S = 1$. The crosses indicate numerically calculated points on the boundary curves $Q = Q_{c1}(G)$ and $Q = Q_{c2}(G)$

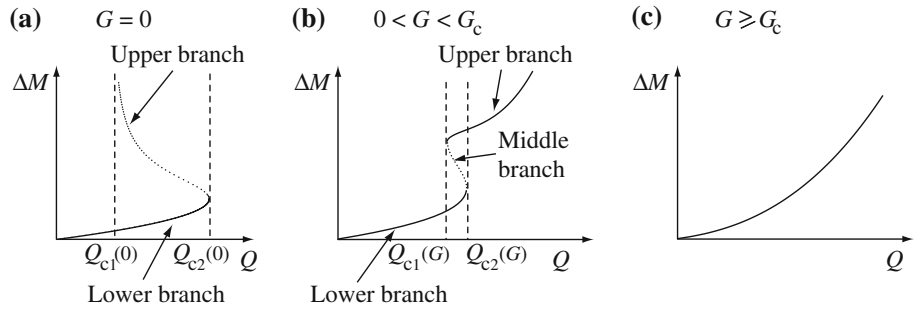

Fig. 3 Sketches of the mass difference per unit width ΔM given by (30) as a function of Q, showing the existence of either none, one, two or three solutions, depending on the values of G and Q. Linearly stable branches are shown with a full line and linearly unstable branches with a dotted line

lying in the interval $0 < Q \leq Q_{c1}(0)$, where $Q_{c1}(0) \simeq 0.601$, there are two solutions for values of Q lying in the interval $Q_{c1}(0) < Q < Q_{c2}(0)$, where $Q_{c2}(0) \simeq 0.708$, there is one solution when $Q = Q_{c2}(0)$, and there is no solution for values of Q satisfying $Q > Q_{c2}(0)$. These results are consistent with those of Moriarty and Terrill [5]. If $G \neq 0$, there are two possibilities. On the one hand, if $0 < G < G_c$, where $G_c \simeq 0.184$, there are either one, two or three solutions, depending on the value of Q; specifically, there exist critical values of the flux $Q_{c1} = Q_{c1}(G)$ and $Q_{c2} = Q_{c2}(G)$ such that there is a unique solution for values of Q lying in the interval $0 < Q < Q_{c1}(G)$, there are two solutions when $Q = Q_{c1}(G)$, there are three solutions for values of Q lying in the interval $Q_{c1}(G) < Q < Q_{c2}(G)$, there are two solutions when $Q = Q_{c2}(G)$, and there is again a unique solution for values of Q satisfying $Q > Q_{c2}(G)$. On the other hand, if $G \geq G_c$, there is a unique solution for all values of Q. Note that, as Fig. 2 shows, $Q_{c1}(G_c) = Q_{c2}(G_c) = Q_c \simeq 0.720$. Furthermore, Fig. 2 also shows that, when either G is sufficiently large (specifically when $G \geq G_c$) and/or Q is sufficiently large (specifically when $Q \geq Q_c$), there is always a unique solution. Note that when multiple solutions occur they are identical under and downstream of the blade, but differ upstream of it.

The difference in the (non-dimensional) mass per unit width between the film upstream of the blade and a uniform film of thickness Q, that is,

$$\Delta M = \int_{-\infty}^{0} (h - Q)\,\mathrm{d}x, \tag{30}$$

where mass has been non-dimensionalised with ρBL, is a useful integral measure of the steady solutions. Figure 3 shows sketches of ΔM as a function of Q for $G = 0$, $0 < G < G_c$ and $G \geq G_c$, and again illustrates that the number

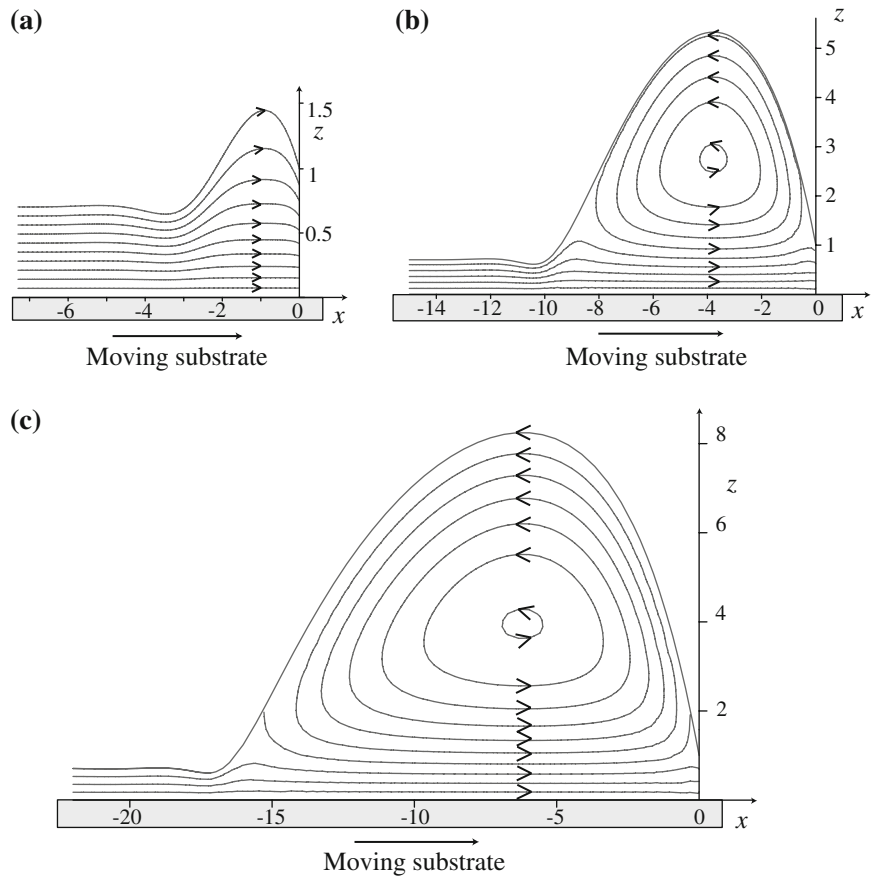

Fig. 4 Upstream streamlines when $b = 1$, $p_{\infty \mathrm{L}} = p_{\infty \mathrm{R}}$, $S = 1$, $G = 0.1$ and $Q = 0.705$, parameter values for which there are three solutions

of solutions that exist depends on the values of G and Q. The stability results included in Fig. 3 are discussed in Sect. 2.3 below.

Figures 4 and 5 show the free-surface profiles and streamline patterns upstream and downstream of the blade, respectively, when $b = 1$, $p_{\infty \mathrm{L}} = p_{\infty \mathrm{R}}$, $S = 1$, $G = 0.1$ and $Q = 0.705$, parameter values for which there are three solutions. The solutions in Fig. 4a, b and c lie on the lower, middle and upper branches in Fig. 3b, respectively. In particular, Fig. 4 shows that for these particular parameter values, there is no reverse flow for the solution on the lower branch, whereas for the solutions on the middle and upper branches there is a region of reverse flow when $h > 3Q = 2.115$. Figure 5 shows that, for these particular parameter values, there is no reverse flow downstream of the blade.

The solutions in the asymptotic limits $Q \to 0$, $Q \to \infty$, $G \to 0$ and $G \to \infty$ are of particular interest (not least because they are difficult to calculate numerically) and will be described in detail in Sects. 3–5 below, respectively. However, before determining the solutions in these asymptotic limits, we investigate the stability of the steady solutions described above in the next subsection.

2.3 Stability of the steady solutions

The typical characteristics of most coating processes (such as high-speed operation, non-Newtonian fluids, external pollutants, contaminants in the coating fluid or on the substrate, machine vibrations or extreme temperatures) mean

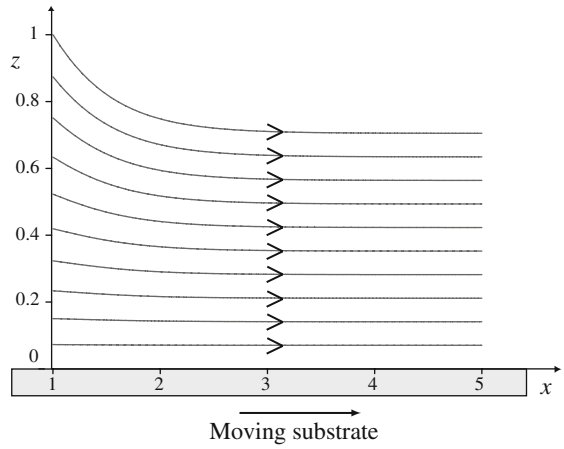

Fig. 5 Downstream streamlines when $b = 1$, $p_{\infty \mathrm{L}} = p_{\infty \mathrm{R}}$, $S = 1$, $G = 0.1$ and $Q = 0.705$

that they are typically subject to various instabilities, such as "ribbing" and "fingering" (see, for example, [1] and [2]).

A linear stability analysis using the standard approach pioneered by Troian et al. [11] and used extensively by many other authors for a wide range of thin-film flows (see, for example, [12]) described by Quintans Carou [13] strongly suggests that solutions on the upper branch in Fig. 3a and the middle branch in Fig. 3b are linearly unstable, but that solutions on the other branches in Fig. 3 are linearly stable. As Quintans Carou [13] describes, this unexpectedly subtle analysis is surprisingly similar to that for a moving pressure disturbance on a thin film on an inclined plane performed by Kriegsmann et al. [14]. In particular, the stability of solutions on an infinite domain (as opposed to the large-but-finite domains used in the numerical calculations) remains open. Quintans Carou [13] also examined both the energy and the rate of dissipation of the steady solutions, but the results were inconclusive and so are not discussed any further here.

Support for the linear stability results in the special case of two-dimensional perturbations can be obtained by calculating the nonlinear temporal evolution of the unsteady (but still two-dimensional) version of the present problem (for which, of course, the flux no longer takes a constant value) by solving

$$h_t + \left[\frac{h^3}{3}(Sh_{xx} - Gh)_x + h\right]_x = 0, \tag{31}$$

where time t has been non-dimensionalised with L/U, subject to the boundary conditions (7), (8), (13), (29) and continuity of flux in the x-direction at the ends of the blade. These calculations were undertaken using a finite-element method implemented via the MATLAB-based numerical analysis package FEMLAB (now called COMSOL) [15], using the static solution when the substrate is at rest (i.e., when $U = 0$) as the initial condition at $t = 0$. When $G = 0$ this initial condition is given by

$$h = \begin{cases} b_0 + \dfrac{(b_0 - Q)}{L_\mathrm{d}^2} x(x + 2L_\mathrm{d}) & \text{for } -L_\mathrm{d} \le x \le 0, \\ b_1 + \dfrac{(b_1 - Q)}{L_\mathrm{d}^2}(x-1)(x - 1 - 2L_\mathrm{d}) & \text{for } 1 \le x \le 1 + L_\mathrm{d}, \end{cases} \tag{32}$$

where L_d is the length of the computational domain upstream and downstream of the blade, and when $G \neq 0$ it is given by

$$h = \begin{cases} Q + (b_0 - Q)\exp\left(\sqrt{\dfrac{G}{S}}x\right) & \text{for } -L_\mathrm{d} \le x \le 0, \\ Q + (b_1 - Q)\exp\left(-\sqrt{\dfrac{G}{S}}(x-1)\right) & \text{for } 1 \le x \le 1 + L_\mathrm{d}. \end{cases} \tag{33}$$

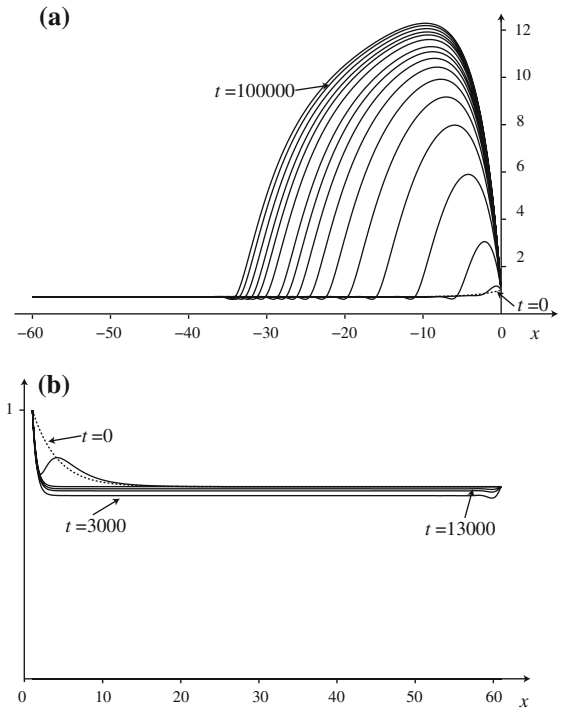

Fig. 6 Evolution from the static solution when the substrate is at rest (**a**) upstream and (**b**) downstream of the blade when $b = 1$, $p_{\infty L} = p_{\infty R}$, $S = 1$, $G = 0.1$ and $Q = 0.715$, parameter values for which there is one steady solution. Times shown are $t = 1{,}000$ to $10{,}000$ (in steps of $1{,}000$), $t = 12{,}000$ to $t = 16{,}000$ (in steps of $2{,}000$), $t = 20{,}000$ and $t = 100{,}000$ upstream of the blade, and $t = 1{,}000$–$13{,}000$ (in steps of $4{,}000$) downstream of the blade. The initial state is shown with a dashed line and the steady solution with a thick line

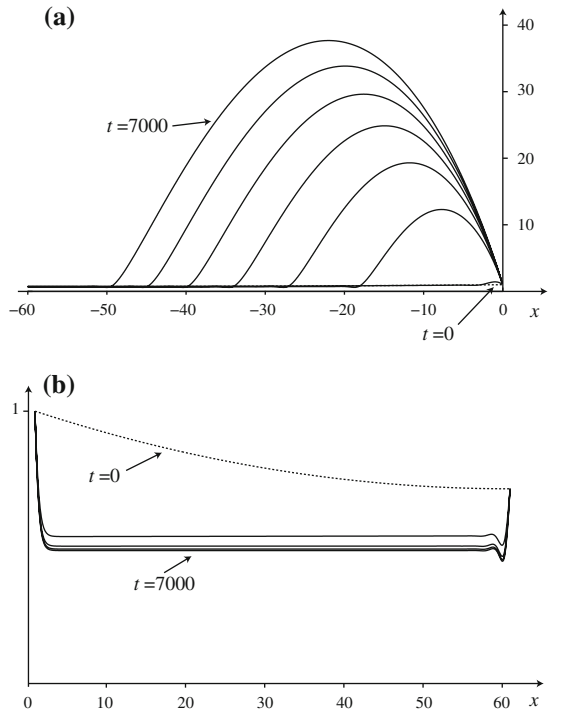

Fig. 7 Evolution from the static solution when the substrate is at rest (**a**) upstream and (**b**) downstream of the blade when $b = 1$, $p_{\infty L} = p_{\infty R}$, $S = 1$, $G = 0$ and $Q = 0.715$, parameter values for which there is no steady solution. Times shown are $t = 1{,}000$–$7{,}000$ (in steps of $1{,}000$ upstream of the blade and in steps of $2{,}000$ downstream of the blade). The initial state is shown with a dashed line

The substrate was started impulsively at $t = 0$ with constant (nondimensional) speed unity and the subsequent evolution determined. The results of these unsteady calculations are entirely consistent with those of the linear stability analysis. For example, on the one hand, Fig. 6 shows the evolution in a case when $G = 0.1 < G_c \simeq 0.184$ and $Q = 0.715 > Q_{c2}(G) \simeq 0.714$ from the static solution (shown with a dashed line) towards the unique steady solution on the upper branch in Fig. 3b (shown with a thick line). On the other hand, Fig. 7 shows the evolution in a case when $G = 0$ and $Q = 0.715 > Q_{c2}(0) \simeq 0.708$ from the static solution (again shown with a dashed line). In this case there is no steady solution and the thickness of the film upstream of the blade increases without bound while the thickness of the film downstream of the blade decreases with t. In all the stable cases investigated the free surface evolved from the static solution towards the lowest branch solution (i.e., the solution with the lowest value of ΔM) available.

3 Solution in the limit $Q \to 0$

In this section we study the solution in the asymptotic limit of small flux, i.e., in the limit $Q \to 0$, in which the film is thin and flat, except near to the ends of the blade where a narrow "meniscus" forms. In the limit $Q \to 0$ the solutions both upstream and downstream of the blade have three asymptotic regions: an "outer" region away from the blade in which the thickness of the film is $O(Q)$ and a narrow "inner" region near the blade of width $O(\sqrt{Q})$ in which the thickness of the film is $O(1)$, connected via an even narrower "transition" region of width $O(Q)$ in

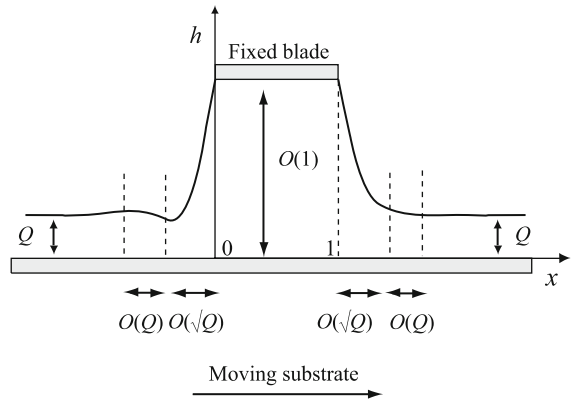

Fig. 8 Sketch of the asymptotic solution in the limit $Q \to 0$

which the thickness of the film rapidly adjusts from its $O(Q)$ outer values to its $O(1)$ inner values. The form of the asymptotic solution in the limit $Q \to 0$ is sketched in Fig. 8.

In the upstream transition region gravity is negligible. Writing

$$x = -x_0 + Q\hat{x}, \quad h = Q\hat{h}, \tag{34}$$

where $x = -x_0$ is the unknown leading-order position of the upstream transition region, we find that at leading-order equation (27) reduces to the well-known Landau–Levich equation (see, for example [16] and [17]) given by

$$S\hat{h}_{\hat{x}\hat{x}\hat{x}} = \frac{3(1-\hat{h})}{\hat{h}^3}, \tag{35}$$

which must be solved numerically subject to the appropriate matching conditions with the outer solution as $\hat{x} \to -\infty$, i.e., $\hat{h} \to 1$ as $\hat{x} \to -\infty$, and with the inner solution as $\hat{x} \to \infty$. The appropriate behaviour of $\hat{h}$ as $\hat{x} \to \infty$ is

$$\hat{h} \sim \frac{c_0}{2}\hat{x}^2, \tag{36}$$

where c_0 is an unknown constant, and $\hat{h}$ approaches unity in an oscillatory manner as $\hat{x} \to -\infty$ according to

$$\hat{h} - 1 \propto \exp\left[\frac{1}{2}\left(\frac{3}{S}\right)^{\frac{1}{3}}\hat{x}\right]\cos\left[\frac{\sqrt{3}}{2}\left(\frac{3}{S}\right)^{\frac{1}{3}}\hat{x} + \phi\right], \tag{37}$$

where ϕ is an unknown phase shift (see, for example, [17]).

In the upstream inner region near $x = 0$ surface tension is dominant. Writing

$$x = \sqrt{Q}\tilde{x}, \quad h = \tilde{h}, \tag{38}$$

we find that at leading order Eq. 27 reduces to simply

$$\tilde{h}_{\tilde{x}\tilde{x}\tilde{x}} = 0, \tag{39}$$

which can be solved explicitly subject to the appropriate matching conditions with the upstream transition solution at $x = -x_0 = -\sqrt{Q}\tilde{x}_0$, i.e., $\tilde{h}(-\tilde{x}_0) = 0$, $\tilde{h}_{\tilde{x}}(-\tilde{x}_0) = 0$ and $\tilde{h}_{\tilde{x}\tilde{x}}(-\tilde{x}_0) = c_0$, to yield the leading-order upstream inner solution, namely

$$\tilde{h} = \frac{c_0}{2}(\tilde{x} + \tilde{x}_0)^2. \tag{40}$$

Since $\tilde{h}(0) = b_0$, we find that x_0 is given by

$$x_0 = \sqrt{\frac{2b_0 Q}{c_0}}. \tag{41}$$

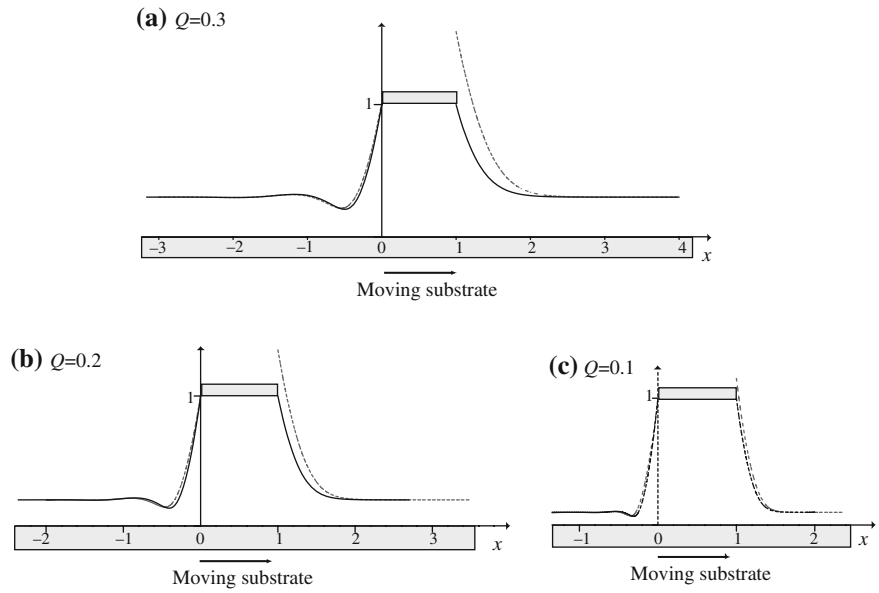

Fig. 9 Free-surface profile h computed numerically (marked with a full line) and the composite leading-order asymptotic solution (47) in the limit $Q \to 0$ (marked with a dashed line) when $b = 1$, $p_{\infty \mathrm{L}} = p_{\infty \mathrm{R}}$ and $S = G = 1$ for (**a**) $Q = 0.3$, (**b**) $Q = 0.2$ and (**c**) $Q = 0.1$

As Quintans Carou [13] describes, similar arguments apply downstream of the blade. Writing

$$x = x_1 + Q\hat{x}, \quad h = Q\hat{h}, \tag{42}$$

where $x = x_1$ is the unknown leading-order position of the downstream transition region, we obtain the appropriate behaviour of $\hat{h}$ in the downstream transition region as $\hat{x} \to -\infty$:

$$\hat{h} \sim \frac{c_1}{2}\,\hat{x}^2, \tag{43}$$

where (unlike in the upstream transition region) the value of the constant c_1 can be determined by solving the Landau–Levich equation (35) numerically, and $\hat{h}$ approaches unity in a monotonic manner as $\hat{x} \to +\infty$ according to

$$\hat{h} - 1 \propto \exp\left[-\left(\frac{3}{S}\right)^{\frac{1}{3}}\hat{x}\right] \tag{44}$$

(see, for example, [17]). Proceeding as before, we find that x_1 is given by

$$x_1 = 1 + \sqrt{\frac{2b_1 Q}{c_1}}. \tag{45}$$

Finally, imposing the continuity-of-pressure condition (29) determines c_0 to be equal to c_1.

The leading-order mass difference per unit width ΔM defined by (30) is given by

$$\Delta M = \frac{\sqrt{Q}c_0\tilde{x}_0^3}{6} = O\left(\sqrt{Q}\right) \to 0. \tag{46}$$

A uniformly valid composite leading-order asymptotic solution for h is

$$h = Q \times \begin{cases} \hat{h}\left(\dfrac{x + x_0}{Q}\right) & \text{for } x \le 0, \\ \hat{h}\left(\dfrac{x - x_1}{Q}\right) & \text{for } x \ge 1, \end{cases} \tag{47}$$

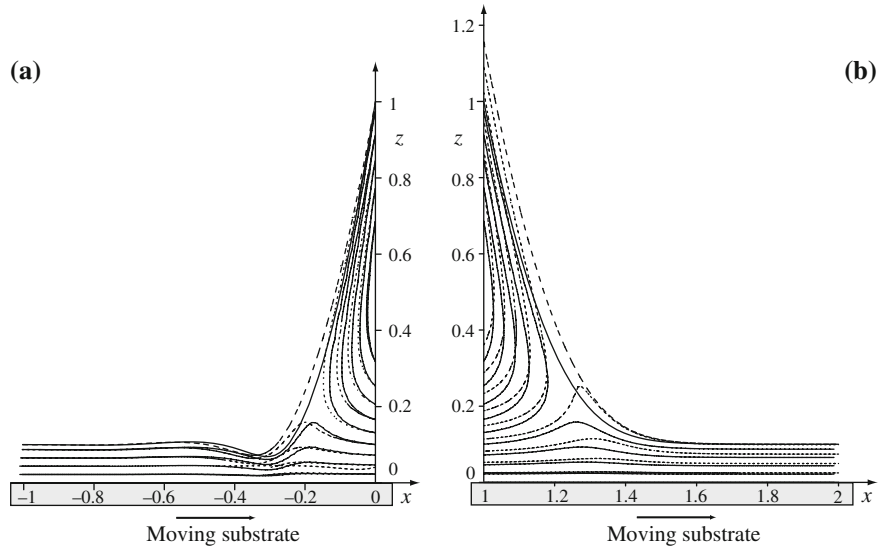

Fig. 10 Streamlines computed numerically (marked with full lines) and using the composite leading-order asymptotic solution (47) in the limit $Q \to 0$ (marked with dashed lines) when $b = 1$, $p_{\infty \mathrm{L}} = p_{\infty \mathrm{R}}$, $S = G = 1$ and $Q = 0.1$

where $\hat{h}$ is the appropriate solution to the Landau–Levich equation (35) upstream and downstream of the blade, respectively. Figure 9 shows the free-surface profile h computed numerically (marked with a full line) and the composite leading-order asymptotic solution (47) (marked with a dashed line) when $b = 1$, $p_{\infty \mathrm{L}} = p_{\infty \mathrm{R}}$ and $S = G = 1$ for various values of Q.

A uniformly valid composite leading-order asymptotic stream function ψ is given by (26) with h given by the composite leading-order asymptotic solution (47). Since reverse flow occurs when $h > 3Q$ and the thickness of the film is $O(1)$ near the blade, there are always regions of reverse flow near the ends of the blade in the limit $Q \to 0$. Figure 10 shows streamlines computed numerically (marked with full lines) and using the composite leading-order asymptotic solution (47) (marked with dashed lines) when $b = 1$, $p_{\infty \mathrm{L}} = p_{\infty \mathrm{R}}$, $S = G = 1$ and $Q = 0.1$, confirming that reverse flow occurs when $h > 3Q = 0.3$.

4 Solution in the limit $Q \to \infty$

In this section we study the solution in the asymptotic limit of large flux, i.e., in the limit $Q \to \infty$, in which there is a large "pile up" of fluid upstream of the blade. In the limit $Q \to \infty$ the solution upstream of the blade has three asymptotic regions: an "outer" region away from the blade of width $O(Q^3)$ in which the thickness of the film is $O(Q)$ and a narrow "inner" region near the blade of width $O(1/\sqrt{Q})$ in which the thickness of the film is $O(1)$, connected via a "transition" region of width $O(1)$ in which the thickness of the film adjusts from its $O(Q)$ outer values to its $O(1)$ inner values. Downstream of the blade there are only two asymptotic regions: an "outer" region in which the thickness of the film is $O(Q)$ and a narrow "inner" region near the blade of width $O(1/\sqrt{Q})$ in which the thickness of the film is $O(1)$. The form of the asymptotic solution in the limit $Q \to \infty$ is sketched in Fig. 11.

In the upstream outer region surface tension is negligible. Writing

$$x = Q^3 \hat{x}, \quad h = Q\hat{h}, \tag{48}$$

we find that at leading order Eq. 27 reduces to

$$-G\,\hat{h}_{\hat{x}} = \frac{3(1-\hat{h})}{\hat{h}^3}, \tag{49}$$

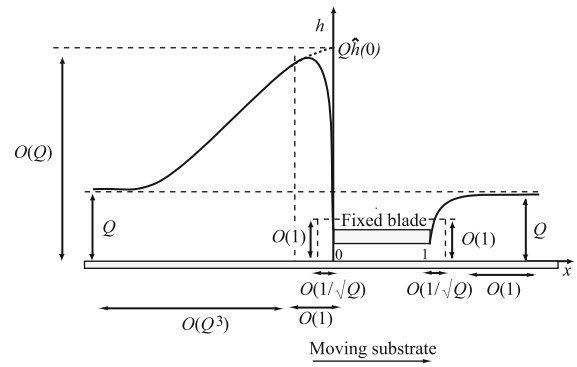

Fig. 11 Sketch of the asymptotic solution in the limit $Q \to \infty$

and hence the leading-order upstream outer solution is given implicitly by

$$\frac{\hat{h}^3}{3} + \frac{\hat{h}^2}{2} + \hat{h} + \log(\hat{h} - 1) = \frac{3}{G}(\hat{x} + \hat{x}_0), \tag{50}$$

and hence the unknown constant $\hat{x}_0$ is given in terms of $\hat{h}(0)$ by

$$\hat{x}_0 = \frac{G}{3}\left\{\frac{\hat{h}(0)^3}{3} + \frac{\hat{h}(0)^2}{2} + \hat{h}(0) + \log[\hat{h}(0) - 1]\right\}. \tag{51}$$

In the transition region surface tension and gravity are dominant. Writing

$$x = \tilde{x}, \quad h = Q\tilde{h}, \tag{52}$$

we find that at leading order Eq. 27 reduces to

$$(S\tilde{h}_{\tilde{x}\tilde{x}} - G\tilde{h})_{\tilde{x}} = 0, \tag{53}$$

which can be solved explicitly subject to the appropriate matching conditions with the upstream inner solution at $\tilde{x} = 0$, i.e., $\tilde{h}(0) = 0$, and with the upstream outer solution as $\tilde{x} \to -\infty$, i.e., $\tilde{h} \to \hat{h}(0)$ as $\tilde{x} \to -\infty$, to yield the leading-order transition solution, namely

$$\tilde{h} = \hat{h}(0)\left[1 - \exp\left(\sqrt{\frac{G}{S}}\tilde{x}\right)\right]. \tag{54}$$

The transition solution (54) does not satisfy the correct boundary condition at the left hand end of the blade, and this is achieved via the upstream inner region in which surface tension is dominant. Writing

$$x = \frac{\bar{x}}{\sqrt{Q}}, \quad h = \bar{h}, \tag{55}$$

we find that at leading order Eq. 27 reduces to simply

$$\bar{h}_{\bar{x}\bar{x}\bar{x}} = 0, \tag{56}$$

which can be solved explicitly subject to the boundary condition $\bar{h}(0) = b_0$ and the appropriate matching condition with the transition solution as $\bar{x} \to -\infty$. However, the leading-order value of h_{xx} is constant throughout the inner region, and so it is not necessary to calculate this solution in order to determine the leading order contribution to the continuity-of-pressure condition (29) from the upstream flow; therefore we do not consider it any further here.

In the downstream outer region surface tension and gravity are dominant everywhere. Writing

$$x = 1 + \hat{x}, \quad h = Q\hat{h}, \tag{57}$$

we find that at leading order Eq. 27 reduces to

$$(S\hat{h}_{\hat{x}\hat{x}} - G\hat{h})_{\hat{x}} = 0, \tag{58}$$

which can be solved explicitly subject to the appropriate matching conditions with the downstream inner solution at $\hat{x} = 0$, i.e., $\hat{h}(0) = 0$, and with the uniform film as $\hat{x} \to \infty$, i.e., $\hat{h} \to 1$ as $\hat{x} \to \infty$, to yield the leading-order downstream outer solution, namely

$$\hat{h} = 1 - \exp\left(-\sqrt{\frac{G}{S}}\hat{x}\right). \tag{59}$$

The downstream outer solution (59) does not satisfy the correct boundary condition at the right-hand end of the blade, and this is achieved via the downstream inner region in which surface tension is dominant. However, as for the upstream inner region, it is not necessary to calculate this solution in order to determine the leading-order contribution to the continuity-of-pressure condition (29) from the downstream flow.

Finally, imposing the continuity-of-pressure condition (29) determines $\hat{h}(0)$ to be

$$\hat{h}(0) = 1 + \frac{12I_3(1)}{G}, \tag{60}$$

where $\hat{h}$ is given implicitly by (50) and $I_3(1)$ is given by (18).

The leading-order mass difference per unit width ΔM defined by (30) is given by

$$\Delta M = \frac{GQ^4\left[\hat{h}(0)^4 - 1\right]}{12} = O\left(Q^4\right) \to \infty. \tag{61}$$

A composite leading-order asymptotic solution for h (uniformly valid everywhere except in the inner regions) is

$$h = Q \times \begin{cases} \hat{h}\left(\dfrac{x}{Q^3}\right) - \hat{h}(0)\exp\left(\sqrt{\dfrac{G}{S}}x\right) & \text{for } x \le 0, \\ 1 - \exp\left(-\sqrt{\dfrac{G}{S}}(x-1)\right) & \text{for } x \ge 1, \end{cases} \tag{62}$$

where $\hat{h}$ is given implicitly by (50) and $\hat{h}(0)$ is given by (60). Figures 12 and 13 show the upstream and downstream free-surface profiles h, respectively, computed numerically (marked with a full line) and the composite leading-order asymptotic solution (62) (marked with a dashed line) when $p_{\infty \mathrm{L}} = p_{\infty \mathrm{R}}$ and $S = G = 1$ for various values of Q for $b = 2$ and $b = 1$, respectively.

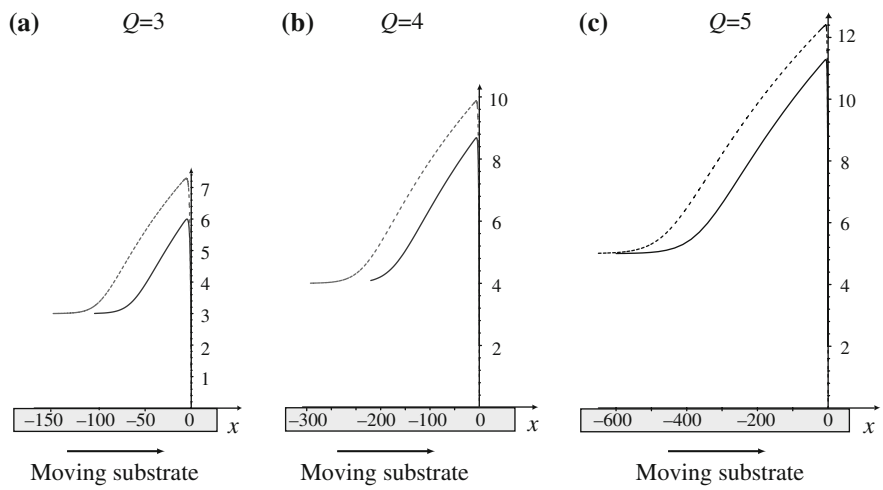

Fig. 12 Upstream free-surface profile h computed numerically (marked with a full line) and the composite leading-order asymptotic solution (62) in the limit $Q \to \infty$ (marked with a dashed line) when $b = 2$, $p_{\infty \mathrm{L}} = p_{\infty \mathrm{R}}$ and $S = G = 1$ for (**a**) $Q = 3$, (**b**) $Q = 4$ and (**c**) $Q = 5$

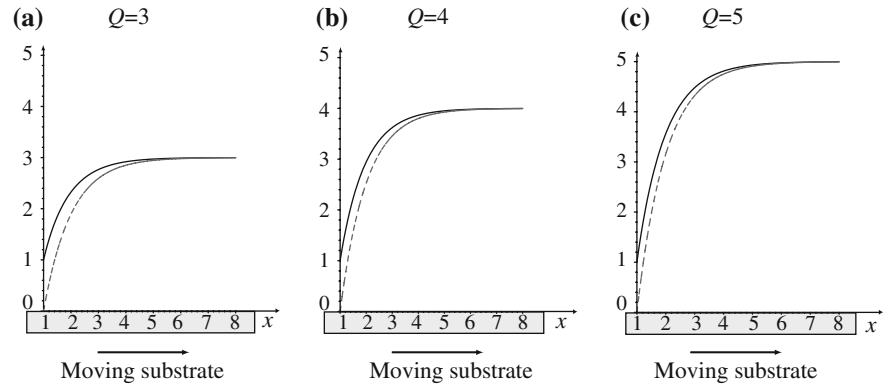

Fig. 13 Downstream free-surface profile h computed numerically (marked with a full line) and the composite leading-order asymptotic solution (62) in the limit $Q \to \infty$ (marked with a dashed line) when $b = 1$, $p_{\infty \mathrm{L}} = p_{\infty \mathrm{R}}$ and $S = G = 1$ for (**a**) $Q = 3$, (**b**) $Q = 4$ and (**c**) $Q = 5$

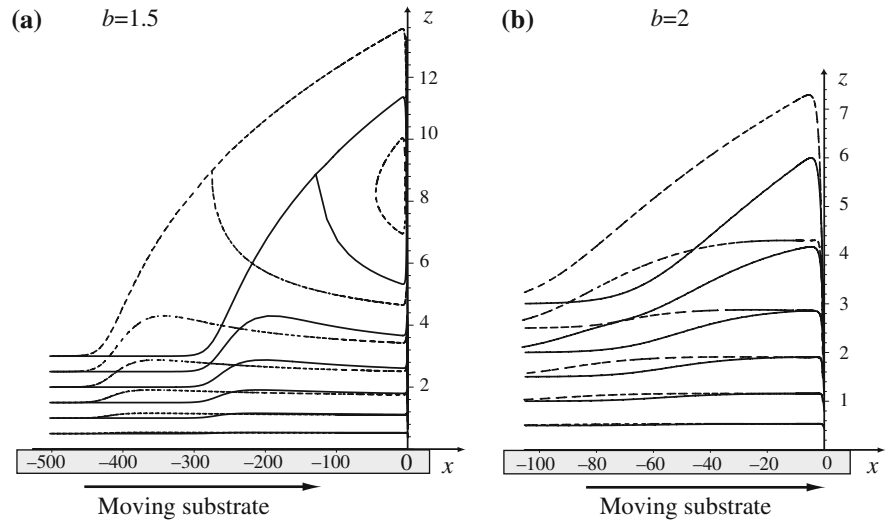

Fig. 14 Upstream streamlines computed numerically (marked with full lines) and using the composite leading-order asymptotic solution (62) in the limit $Q \to \infty$ (marked with dashed lines) when $p_{\infty \mathrm{L}} = p_{\infty \mathrm{R}}$, $S = G = 1$ and $Q = 3$ for (**a**) $b = 1.5$ and (**b**) $b = 2$

In the upstream outer region the leading-order outer stream function $\hat{\psi}$ is

$$\hat{\psi} = \frac{3\left(\hat{h}-1\right)}{2\hat{h}^3}\left(\frac{\hat{z}^3}{3} - \hat{h}\hat{z}^2\right) + \hat{z}, \tag{63}$$

where $z = Q\hat{z}$, $\psi = Q\hat{\psi}$, and $\hat{h}$ is given implicitly by (50). From (63) we see that $u = 0$ on the curve $\hat{z} = \hat{z}_0$, where $\hat{z}_0$ is given by

$$\frac{\hat{z}_0}{\hat{h}} = 1 - \sqrt{\frac{3-\hat{h}}{3\left(1-\hat{h}\right)}}; \tag{64}$$

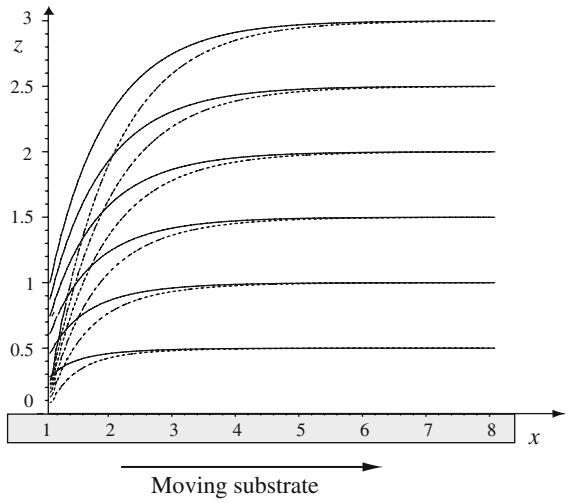

Fig. 15 Downstream streamlines computed numerically (marked with full lines) and using the composite leading-order asymptotic solution (62) in the limit $Q \to \infty$ (marked with dashed lines) when $b = 1$, $p_{\infty \mathrm{L}} = p_{\infty \mathrm{R}}$, $S = G = 1$ and $Q = 3$

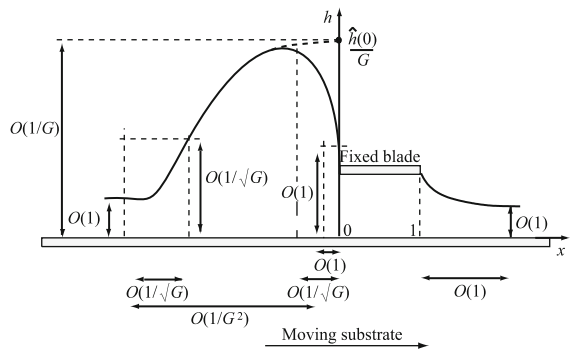

Fig. 16 Sketch of the asymptotic solution in the limit $G \to 0$

thus there is a region of reverse flow between $\hat{z} = \hat{z}_0$ and the free surface $\hat{z} = \hat{h}$ when $\hat{h}(0) > 3$, and the leading-order circulation within the eddy that occurs is equal to $Q(\hat{\psi}_{\max} - 1)$, where $\hat{\psi}_{\max} = \hat{\psi}(0, \hat{z}_0)$, i.e.,

$$\frac{Q\left[\hat{h}(0) - 3\right]}{3} \sqrt{\frac{\hat{h}(0) - 3}{3\left[\hat{h}(0) - 1\right]}} = O(Q) \to \infty. \tag{65}$$

A leading-order asymptotic stream function ψ (uniformly valid everywhere except in the inner regions) is given by (26) with h given by the composite leading-order asymptotic solution (62). Figures 14 and 15 show the upstream and downstream streamlines, respectively, computed numerically (marked with full lines) and using the composite leading-order asymptotic solution (62) (marked with dashed lines) when $p_{\infty \mathrm{L}} = p_{\infty \mathrm{R}}$, $S = G = 1$ and $Q = 3$ for $b = 1.5$ (for which there is reverse flow) and $b = 2$ (for which there is no reverse flow), and for $b = 1$, respectively.

5 Solution in the limit $G \to 0$

In this section we study the upper-branch solution in the asymptotic limit of weak gravity effects, i.e., in the limit $G \to 0$, in which there is a large "pile up" of fluid upstream of the blade. (Note that in this limit the middle- and lower-branch solutions simply approach the upper- and lower-branch solutions in the case $G = 0$, and so are not considered any further here.) In the limit $G \to 0$ the solution upstream of the blade has five asymptotic regions: an "outer outer" region far from the blade in which the thickness of the film is $O(1)$, an "outer" region of width $O(1/G^2)$ in which the thickness of the film is $O(1/G)$, and an "inner" region near the blade of width $O(1)$ in which the thickness of the film is $O(1)$, connected via an "outer transition" region of width $O(1/\sqrt{G})$ in which the thickness of the film adjusts from its $O(1)$ outer outer values to its $O(1/G)$ outer values and an "inner transition" region also of width $O(1/\sqrt{G})$ in which the thickness of the film adjusts from its $O(1/G)$ outer values to its $O(1)$ inner values. Downstream of the blade there is only one region, in which the thickness of the film is $O(1)$. The form of the asymptotic solution in the limit $G \to 0$ is sketched in Fig. 16.

In the upstream outer region gravity and viscous shear are dominant. Writing

$$x = \frac{\hat{x}}{G^2}, \quad h = \frac{\hat{h}}{G}, \tag{66}$$

we find that at leading order Eq. 27 reduces to

$$\hat{h}_{\hat{x}} = \frac{3}{\hat{h}^2}, \tag{67}$$

which can be solved explicitly subject to the appropriate matching condition with the outer transition solution at $x = -x_0 = -\hat{x}_0/G^2$, i.e., $\hat{h}(-\hat{x}_0) = 0$, where $x = -x_0$ is the unknown leading-order position of the outer transition region, to yield the leading-order upstream outer solution, namely

$$\hat{h} = \left[9(\hat{x} + \hat{x}_0)\right]^{1/3}. \tag{68}$$

In the outer transition region near $x = -x_0$ surface tension, gravity and viscous shear are all significant. Writing

$$x = -x_0 + \frac{\bar{x}}{\sqrt{G}}, \quad h = \frac{\bar{h}}{\sqrt{G}}, \tag{69}$$

we find that at leading order Eq. 27 reduces to

$$(S\bar{h}_{\bar{x}\bar{x}} - \bar{h})_{\bar{x}} = -\frac{3}{\bar{h}^2}, \tag{70}$$

which must, in general, be solved numerically. The solution of (70) will match with the leading order outer solution $\hat{h}$ given by (68) as $\bar{x} \to \infty$, but not with the uniform film $h = Q$ as $\bar{x} \to -\infty$, and so this latter matching is achieved in the outer outer region in which gravity is negligible and at leading order Eq. 27 reduces to the Landau–Levich equation. However, since neither the outer transition region nor this outer outer region feed back any information to the outer solution, we do not need to consider them any further here.

In the inner transition region surface tension and gravity are dominant. Writing

$$x = \frac{\tilde{x}}{\sqrt{G}}, \quad h = \frac{\tilde{h}}{G}, \tag{71}$$

we find that at leading order Eq. 27 reduces to

$$(S\tilde{h}_{\tilde{x}\tilde{x}} - \tilde{h})_{\tilde{x}} = 0, \tag{72}$$

which can be solved explicitly subject to the appropriate matching conditions with the inner solution at $\tilde{x} = 0$, i.e., $\tilde{h}(0) = 0$, and with the outer solution as $\tilde{x} \to -\infty$, i.e., $\tilde{h} \to \hat{h}(0) = (9\hat{x}_0)^{1/3}$ as $\tilde{x} \to -\infty$, to yield the leading-order inner transition solution,

$$\tilde{h} = (9\hat{x}_0)^{1/3}\left[1 - \exp\left(\sqrt{\frac{1}{S}}\tilde{x}\right)\right]. \tag{73}$$

The transition solution (73) does not satisfy the correct boundary condition at the left-hand end of the blade, and this is achieved via the inner region in which surface tension is dominant. However, just like in the limit $Q \to \infty$, the value of h_{xx} is constant over this region, and so it is not necessary to calculate this solution in order to determine the leading-order contribution to the continuity-of-pressure condition (29) from the upstream flow.

Downstream of the blade gravity is negligible everywhere. Writing

$$x = 1 + \hat{x}, \quad h = \hat{h}, \tag{74}$$

we find that at leading order Eq. 27 reduces to the Landau–Levich equation given by

$$S\hat{h}_{\hat{x}\hat{x}\hat{x}} = \frac{3(Q - \hat{h})}{\hat{h}^3}, \tag{75}$$

which must be solved numerically subject to the boundary condition $\hat{h}(0) = b_1$ and the appropriate matching condition with the uniform film as $\hat{x} \to \infty$, i.e., $\hat{h} \to Q$ as $\hat{x} \to \infty$.

Finally, imposing the continuity-of-pressure condition (29) determines $\hat{x}_0$ to be

$$\hat{x}_0 = \frac{1}{9}\left[-6I_2(1) + 12QI_3(1) - Sh_{xx}(1) + p_{\infty\mathrm{R}} - p_{\infty\mathrm{L}}\right]^3, \tag{76}$$

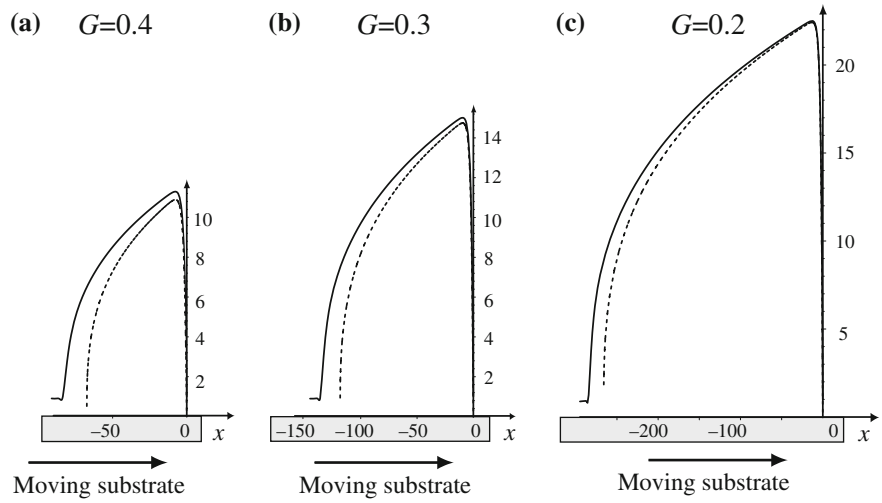

Fig. 17 Upstream free-surface profile h computed numerically (marked with a full line) and the composite leading-order asymptotic solution (78) in the limit $G \to 0$ (marked with a dashed line) when $b = 1$, $p_{\infty \mathrm{L}} = p_{\infty \mathrm{R}}$, $S = 1$ and $Q = 0.9$ for (**a**) $G = 0.4$, (**b**) $G = 0.3$ and (**c**) $G = 0.2$

where $h_{xx}(1)$ is obtained by solving the Landau–Levich equation (75) numerically.

The leading-order mass difference per unit width ΔM defined by (30) is given by

$$\Delta M = \frac{(3^5 \hat{x}_0^4)^{1/3}}{4G^3} = O\left(\frac{1}{G^3}\right) \to \infty. \tag{77}$$

A composite leading-order asymptotic solution for h (uniformly valid in the upstream outer and inner transition regions and everywhere downstream of the blade) is

$$h = \begin{cases} \left[\dfrac{9(x+x_0)}{G}\right]^{1/3} - \left[\dfrac{9x_0}{G}\right]^{1/3} \exp\left(\sqrt{\dfrac{G}{S}}x\right) & \text{for } x \le 0, \\ \hat{h}(x-1) & \text{for } x \ge 1, \end{cases} \tag{78}$$

where $x_0 = \hat{x}_0/G^2$, with $\hat{x}_0$ given by (76), and $\hat{h}$ is the solution of (75). Figures 17 and 18 show the upstream and downstream free-surface profile h, respectively, computed numerically (marked with a full line) and the composite leading-order asymptotic solution (78) (marked with a dashed line) when $b = 1$, $p_{\infty \mathrm{L}} = p_{\infty \mathrm{R}}$, $S = 1$ and $Q = 0.9$ for various values of G.

In the upstream outer region the leading-order outer stream function $\hat{\psi}$ is

$$\hat{\psi} = \frac{3}{2\hat{h}^2}\left(\frac{\hat{z}^3}{3} - \hat{h}\hat{z}^2\right) + \hat{z}, \tag{79}$$

where $z = \hat{z}/G$, $\psi = \hat{\psi}/G$, and $\hat{h}$ is given by (68). Note that at leading order in this particular limit $\hat{\psi}(\hat{z} = \hat{h}) = 0$. From (79) we see that $u = 0$ on the curve $\hat{z} = \hat{z}_0$, where $\hat{z}_0$ is given by

$$\frac{\hat{z}_0}{\hat{h}} = 1 - \frac{1}{\sqrt{3}}; \tag{80}$$

thus there is always a region of reverse flow between $\hat{z} = \hat{z}_0$ and the free surface $\hat{z} = \hat{h}$, and the leading-order circulation within the eddy that occurs is equal to $\hat{\psi}_{\max}/G$, where $\hat{\psi}_{\max} = \hat{\psi}(0, \hat{z}_0)$, i.e.,

$$\frac{\hat{h}(0)}{3\sqrt{3}G} = \frac{(9\hat{x}_0)^{1/3}}{3\sqrt{3}G} = O\left(\frac{1}{G}\right) \to \infty. \tag{81}$$

A leading-order asymptotic stream function ψ (uniformly valid in the upstream outer and inner transition regions and everywhere downstream of the blade) is given by (26) with h given by the composite leading-order asymptotic

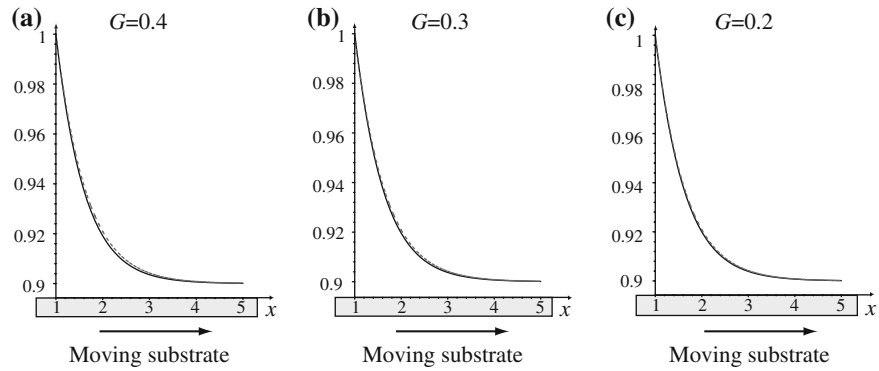

Fig. 18 Downstream free-surface profile h computed numerically (marked with a full line) and the composite leading-order asymptotic solution (78) in the limit $G \to 0$ (marked with a dashed line) when $b = 1$, $p_{\infty \mathrm{L}} = p_{\infty \mathrm{R}}$, $S = 1$ and $Q = 0.9$ for (**a**) $G = 0.4$, (**b**) $G = 0.3$ and (**c**) $G = 0.2$

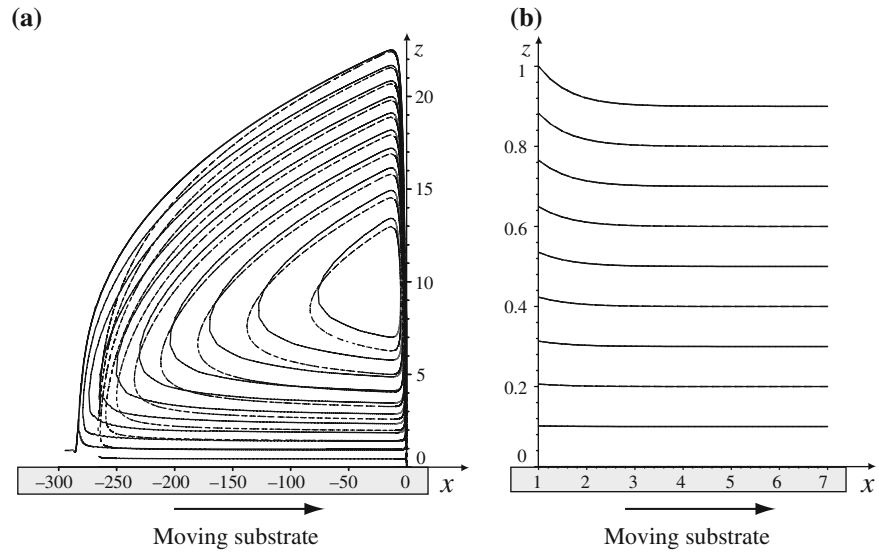

Fig. 19 Streamlines computed numerically (marked with full lines) and using the composite leading-order asymptotic solution (78) in the limit $G \to 0$ (marked with dashed lines) when $b = 1$, $p_{\infty \mathrm{L}} = p_{\infty \mathrm{R}}$, $S = 1$, $G = 0.2$ and $Q = 0.9$. The exact and asymptotic solutions downstream of the blade are indistinguishable for these parameter values

solution (78). Figure 19 shows streamlines computed numerically (marked with full lines) and using the composite leading-order asymptotic solution (78) (marked with dashed lines) when $b = 1$, $p_{\infty \mathrm{L}} = p_{\infty \mathrm{R}}$, $S = 1$, $G = 0.2$ and $Q = 0.9$. In particular, Fig. 19b shows that the convergence of the exact to the asymptotic solution downstream of the blade as $G \to 0$ is so rapid that they are indistinguishable for these parameter values.

6 Solution in the limit $G \to \infty$

In this section we study the solution in the asymptotic limit of strong gravity effects, i.e., in the limit $G \to \infty$, in which the film is flat except near to the ends of the blade where a narrow "meniscus" forms. In the limit $G \to \infty$ the solutions both upstream and downstream of the blade have two asymptotic regions: an "outer" region in which the thickness of the film is $O(1)$ and a narrow "inner" region near the blade of width $O(1/\sqrt{G})$ in which the thickness

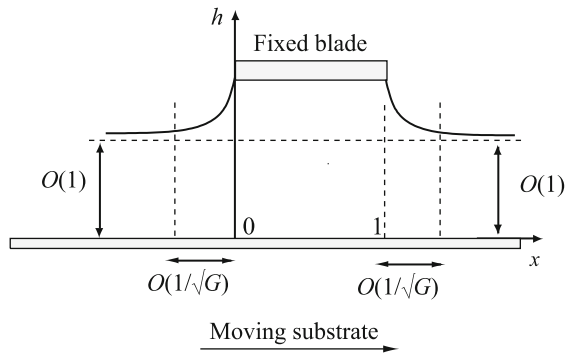

Fig. 20 Sketch of the asymptotic solution in the limit $G \to \infty$

of the film rapidly adjusts from its $O(1)$ value at the end of the blade to its $O(1)$ outer values. The form of the asymptotic solution in the limit $G \to \infty$ is sketched in Fig. 20.

In the upstream inner region surface tension and gravity are dominant. Writing

$$x = \frac{\hat{x}}{\sqrt{G}}, \quad h = \hat{h}, \tag{82}$$

we find that at leading order Eq. 27 reduces to

$$(S\hat{h}_{\hat{x}\hat{x}} - \hat{h})_{\hat{x}} = 0, \tag{83}$$

which can be solved explicitly subject to the boundary condition $\hat{h}(0) = b_0$ and the appropriate matching condition with the upstream outer solution as $\hat{x} \to -\infty$, i.e., $\hat{h} \to Q$ as $\hat{x} \to -\infty$, to yield the leading-order upstream inner solution, namely

$$\hat{h} = Q + (b_0 - Q)\exp\left(\sqrt{\frac{1}{S}}\hat{x}\right). \tag{84}$$

As Quintans Carou [13] describes, similar arguments apply downstream of the blade, where the leading-order inner solution is

$$\hat{h} = Q + (b_1 - Q)\exp\left(-\sqrt{\frac{1}{S}}\hat{x}\right). \tag{85}$$

Note that imposing the continuity-of-pressure condition (29) yields no new information at leading order, and that (84) and (85) coincide with the static solution when the substrate is at rest in the case $G \neq 0$ given by (33).

The leading-order mass difference per unit width ΔM defined by (30) is given by

$$\Delta M = \sqrt{\frac{S}{G}}(b_0 - Q) = O\left(\frac{1}{\sqrt{G}}\right) \to 0. \tag{86}$$

Figures 21 and 22 show the free-surface profile h upstream and downstream of the blade, respectively, computed numerically (marked with a full line) and the leading-order asymptotic solution (33) (marked with a dashed line) when $b = 1$, $p_{\infty \mathrm{L}} = p_{\infty \mathrm{R}}$, $S = 1$ and $Q = 0.7$ for various values of G.

A uniformly valid leading-order asymptotic stream function ψ is given by (26) with h given by the leading-order asymptotic solution (33). Figures 23 and 24 show the streamlines upstream and downstream of the blade, respectively, computed numerically (marked with full lines) and using the leading-order asymptotic solution (33) (marked with dashed lines) when $b = 1$, $p_{\infty \mathrm{L}} = p_{\infty \mathrm{R}}$, $S = 1$ and $G = 50$ (upstream) and $G = 5$ (downstream) for (a) $Q = 0.3$ (for which there is reverse flow when $h > 3Q = 0.9$) and (b) $Q = 0.7$ (for which there is no reverse flow).

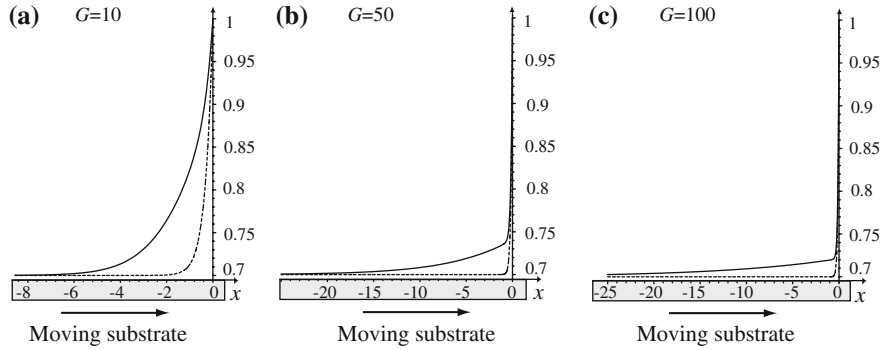

Fig. 21 Upstream free-surface profile h computed numerically (marked with a full line) and the leading-order asymptotic solution (33) in the limit $G \to \infty$ (marked with a dashed line) when $b = 1$, $p_{\infty \mathrm{L}} = p_{\infty \mathrm{R}}$, $S = 1$ and $Q = 0.7$ for (**a**) $G = 10$, (**b**) $G = 50$ and (**c**) $G = 100$

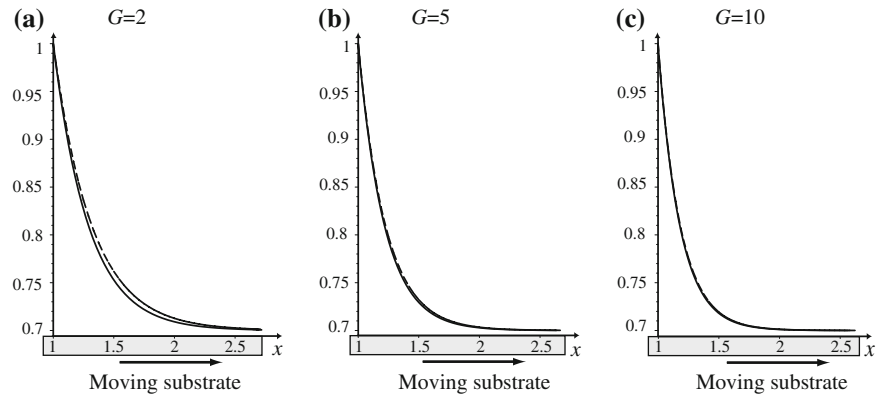

Fig. 22 Downstream free-surface profile h computed numerically (marked with a full line) and the leading-order asymptotic solution (33) in the limit $G \to \infty$ (marked with a dashed line) when $b = 1$, $p_{\infty \mathrm{L}} = p_{\infty \mathrm{R}}$, $S = 1$ and $Q = 0.7$ for (**a**) $G = 2$, (**b**) $G = 5$ and (**c**) $G = 10$

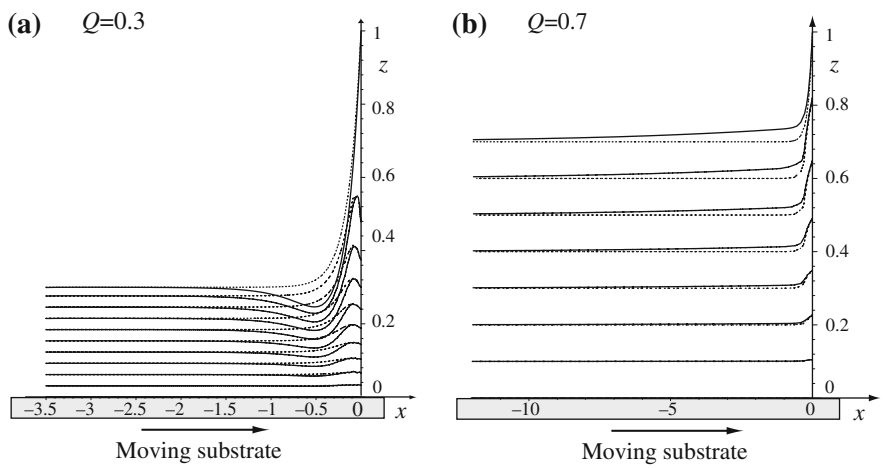

Fig. 23 Upstream streamlines computed numerically (marked with full lines) and using the leading-order asymptotic solution (33) in the limit $G \to \infty$ (marked with dashed lines) when $b = 1$, $p_{\infty \mathrm{L}} = p_{\infty \mathrm{R}}$, $S = 1$ and $G = 50$ for (**a**) $Q = 0.3$ and (**b**) $Q = 0.7$

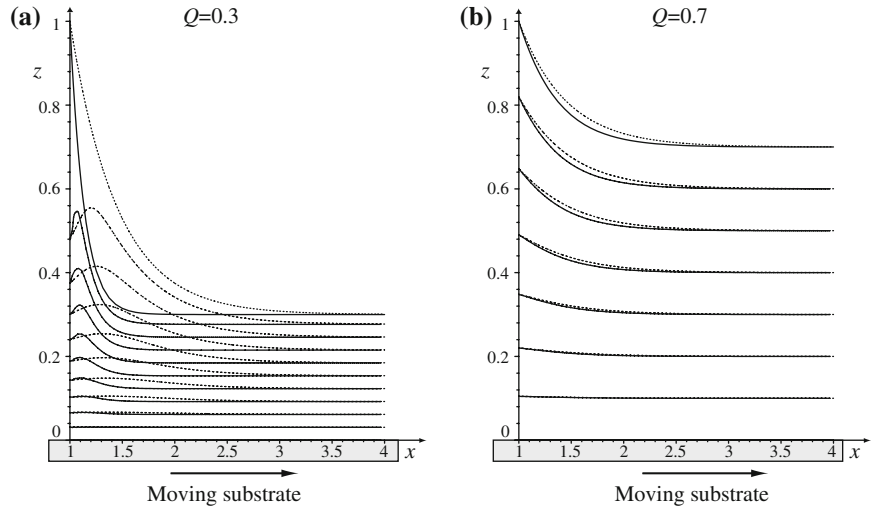

Fig. 24 Downstream streamlines computed numerically (marked with full lines) and using the leading-order asymptotic solution (33) in the limit $G \to \infty$ (marked with dashed lines) when $b = 1$, $p_{\infty \mathrm{L}} = p_{\infty \mathrm{R}}$, $S = 1$ and $G = 5$ for (**a**) $Q = 0.3$ and (**b**) $Q = 0.7$

7 Conclusions

In the present paper we analysed a simple model of the blade-coating process consisting of the flow of a thin film of Newtonian fluid on a horizontal substrate moving parallel to itself with constant speed under a fixed blade of finite length in which the flows upstream and downstream of the blade are coupled via the flow under the blade.

The appropriate solutions for the fluid velocity and pressure under the blade and both upstream and downstream of the blade were found explicitly, and the third-order ordinary differential equation governing the free-surface profile (and associated boundary conditions, one of which couples the solutions upstream and downstream of the blade) was determined.

A combination of asymptotic and numerical methods was used to investigate the number and nature of the steady solutions that exist. In the absence of gravity we obtained results that are consistent with those of Moriarty and Terrill [5]. In the presence of gravity we found that there is always at least one, and (depending on the parameter values) possibly as many as three, steady solutions, and that when multiple solutions occur they are identical under and downstream of the blade, but differ upstream of it.

The stability of these steady solutions was investigated numerically. A linear stability analysis strongly suggests that solutions on the upper branch in Fig. 3a and the middle branch in Fig. 3b are unstable, but that solutions on the other branches in Fig. 3 are stable. Support for the linear stability results in the special case of two-dimensional perturbations was obtained by calculating the nonlinear temporal evolution of the unsteady (but still two-dimensional) version of the present problem. In particular, in all the stable cases investigated the free surface evolved from the static solution towards the lowest branch solution (i.e., the solution with the lowest value of ΔM) available.

The leading-order asymptotic behaviour of the steady solutions in the limits of large and small flux and weak and strong gravity effects, respectively, was examined. These calculations revealed that in the limits $Q \to 0$ and $G \to \infty$ the film is flat except for a narrow "meniscus" near to the ends of the blade, while in the limits $Q \to \infty$ and $G \to 0$ there is a large "pile up" of fluid upstream of the blade. These calculations also revealed that while regions of reverse flow (which might be undesirable in practical coating applications) may or may not occur in the limits $Q \to \infty$ and $G \to \infty$, they always occur both upstream and downstream of the blade in the limit $Q \to 0$ and upstream but not downstream of the blade in the limit $G \to 0$. Furthermore, comparing the exact and asymptotic solutions showed that in most cases the present asymptotic solutions are practically useful and reasonably accurate approximations even when the small parameters are not especially small and the large parameters are not especially large.

Acknowledgements JQC wishes to thank the University of Strathclyde for financial support via a Graduate Teaching Assistantship (2002–06) and a Temporary Assistantship (2006–07).

References

1. Ruschak KJ (1985) Coating flows. Annu Rev Fluid Mech 17:65–89
2. Kistler SF, Schweizer PM (1997) Liquid film coating. Chapman & Hall, London
3. European Coating Symposium 2007 website, www.pmmh.espci.fr/~ecs2007, accessed on 28th February 2008.
4. International Coating Science and Technology Symposium website, www.iscst.org, accessed on 28th February 2008.
5. Moriarty JA, Terrill EL (1996) Mathematical modelling of the motion of hard contact lenses. Eur J Appl Math 7:575–594
6. McLeod JB (1996) Solution of a contact lens problem. Eur J Appl Math 7:595–602
7. Ockendon H, Ockendon JR (1995) Viscous flow. Cambridge University Press, Cambridge
8. Quintans Carou J, Duffy BR, Mottram NJ, Wilson SK (2006) Shear-driven and pressure-driven flow of a nematic liquid crystal in a slowly varying channel. Phys Fluids 18(2):027105-1–027105-13
9. Doedel EJ (1981) AUTO, a program for the automatic bifurcation analysis of autonomous systems. Cong Numer 30:265–384
10. Quintans Carou J, Mottram NJ, Wilson SK, Duffy BR (2007) A mathematical model for blade coating of a nematic liquid crystal. Liq Cryst 34:621–631
11. Troian SM, Herbolzheimer E, Safran SA, Joanny JF (1989) Fingering instabilities of driven spreading films. Europhys Lett 10:25–30
12. Kondic L (2003) Instabilities in gravity driven flow of thin fluid films. SIAM Rev 45:95–115
13. Quintans Carou J (2007) Thin-film flow of liquid crystals. PhD thesis, University of Strathclyde. Available online at www.maths.strath.ac.uk/research/phd_mphil_theses.
14. Kriegsman JJ, Miksis MJ, Vanden-Broeck J-M (1998) Pressure driven disturbances on a thin viscous film. Phys Fluids 10:1249–1255
15. COMSOL website, www.comsol.com, accessed on 28th February 2008.
16. Landau L, Levich VG (1942) Dragging of a liquid by a moving plate. Acta Physicochim (URSS) 17:42–54
17. Tuck EO, Schwartz LW (1990) A numerical and asymptotic study of some third-order ordinary differential equations relevant to draining and coating flows. SIAM Rev 32:453–469